Long-Lived, Non-Geminate, Radiative Recombination of Photogenerated Charges in a Polymer/Small-Molecule Acceptor Photovoltaic Blend

Ziffer, Mark E.; Jo, Sae Byeok; Zhong, Hongliang; Ye, Long; Liu, Hongbin; Lin, Francis; Zhang, Jie; Li, Xiaosong; Ade, Harald W.; Jen, Alex K.-Y.; Ginger, David S.

Published in:
Journal of the American Chemical Society

Published: 08/08/2018

Document Version:
Final Published version, also known as Publisher's PDF, Publisher's Final version or Version of Record

Published version (DOI):
10.1021/jacs.8b05834

Publication details:
Ziffer, M. E., Jo, S. B., Zhong, H., Ye, L., Liu, H., Lin, F., Zhang, J., Li, X., Ade, H. W., Jen, A. K-Y., & Ginger, D. S. (2018). Long-Lived, Non-Geminate, Radiative Recombination of Photogenerated Charges in a Polymer/Small-Molecule Acceptor Photovoltaic Blend. *Journal of the American Chemical Society*, *140*(31), 9996-10008. https://doi.org/10.1021/jacs.8b05834

JACS
JOURNAL OF THE AMERICAN CHEMICAL SOCIETY
Article
Cite This: J. Am. Chem. Soc. 2018, 140, 9996−10008
pubs.acs.org/JACS

Long-Lived, Non-Geminate, Radiative Recombination of Photogenerated Charges in a Polymer/Small-Molecule Acceptor Photovoltaic Blend

Mark E. Ziffer,[†,#] Sae Byeok Jo,[‡,#] Hongliang Zhong,[‡,§] Long Ye,[∥] Hongbin Liu,[†] Francis Lin,[†] Jie Zhang,[†,⊥] Xiaosong Li,[†] Harald W. Ade,[∥] Alex K.-Y. Jen,[*,‡,⊥] and David S. Ginger[*,†]

[†]Department of Chemistry, University of Washington, Seattle, Washington 98195-2120, United States
[‡]Department of Materials Science and Engineering, University of Washington, Seattle, Washington 98195-2120, United States
[§]School of Chemistry and Chemical Engineering, Shanghai Jiao Tong University, Shanghai 200240, China
[∥]Department of Physics and Organic and Carbon Electronics Lab (ORaCEL), North Carolina State University, Raleigh, North Carolina 27695, United States
[⊥]Department of Biology and Chemistry and Department of Physics and Materials Science, City University of Hong Kong, Kowloon, Hong Kong

Supporting Information

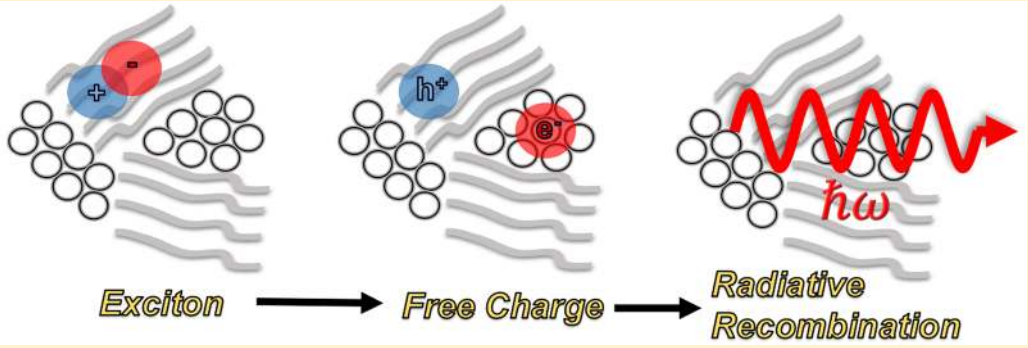

ABSTRACT: Minimization of open-circuit-voltage (V_{OC}) loss is required to transcend the efficiency limitations on the performance of organic photovoltaics (OPV). We study charge recombination in an OPV blend comprising a polymer donor with a small molecule nonfullerene acceptor that exhibits both high photovoltaic internal quantum efficiency and relatively high external electroluminescence quantum efficiency. Notably, this donor/acceptor blend, consisting of the donor polymer commonly referred to as PCE10 with a pseudoplanar small molecule acceptor (referred to as FIDTT-2PDI) exhibits relatively bright delayed photoluminescence on the microsecond time scale beyond that observed in the neat material. We study the photoluminescence decay kinetics of the blend in detail and conclude that this long-lived photoluminescence arises from radiative nongeminate recombination of charge carriers, which we propose occurs via a donor/acceptor CT state located close in energy to the singlet state of the polymer donor. Additionally, crystallographic and spectroscopic studies point toward low subgap disorder, which could be beneficial for low radiative and nonradiative losses. These results provide an important demonstration of photoluminescence due to nongeminate charge recombination in an efficient OPV blend, a key step in identifying new OPV materials and materials-screening criteria if OPV is to approach the theoretical limits to efficiency.

INTRODUCTION

For a solar cell absorber to reach its theoretical maximum efficiency, the following requirements must be met: (1) the material must generate charge efficiently following the absorption of light, and; 2) recombination at open circuit should proceed only via a necessary reciprocal radiative process.[1,2] These arguments, based on the principles of detailed balance,[3] apply to all solar cell materials, from single-crystal GaAs and hybrid perovskites to organic donor/acceptor blend systems. Indeed, eq 1 quantifies the maximum achievable open circuit voltage for a material based on the external luminescence efficiency for free charge recombination (η_{ext}):[4]

$$V_{OC} = V_{OC,ideal} + \frac{kT}{q}\ln(\eta_{ext}) \quad (1)$$

This approach, emphasizing the importance of radiative free charge recombination, has been successfully applied to enhance open circuit voltages and power conversion

Received: June 4, 2018
Published: July 14, 2018

DOI: 10.1021/jacs.8b05834
J. Am. Chem. Soc. 2018, 140, 9996−10008

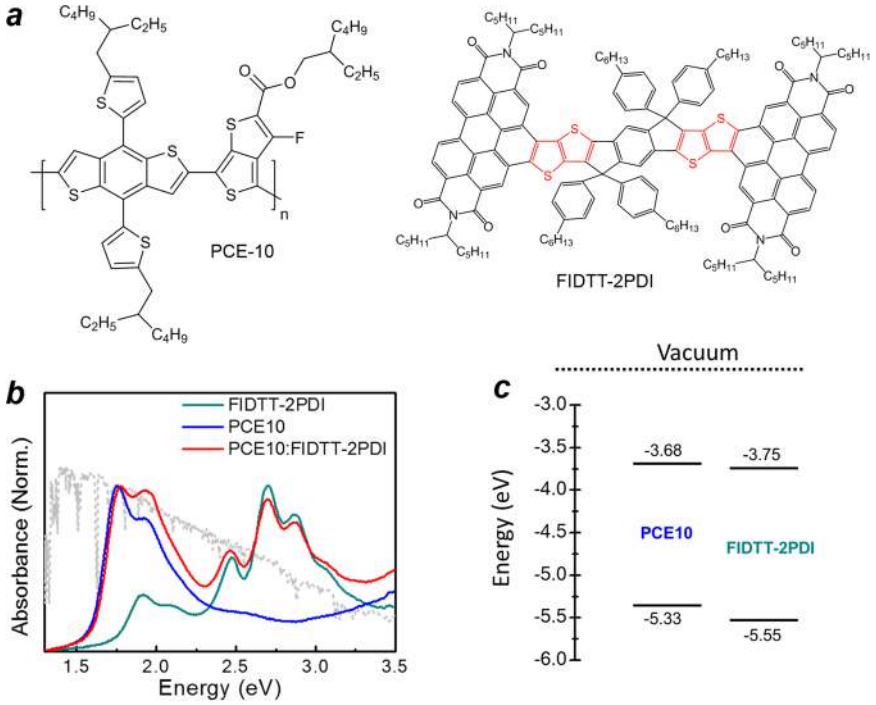

Figure 1. *a* Chemical structures of PCE10 and FIDTT-2PDI. *b* UV−vis absorption spectrum of thin films of PCE10, FIDTT-2PDI, and a 1:1 PCE10:FIDTT-2PDI blend. *c* The energy states (*IE*/IE* and *EA*/EA** for donor and acceptor, respectively)[40] estimated based on the electrochemical energy levels reported in the literature for PCE10[41] and FIDTT-2PDI[42] and their optical bandgaps (see SI Section S13.2 for details). Dotted line in *b* corresponds to AM1.5 global standard solar spectrum (ASTMG173).

efficiencies in a wide range of established and emerging photovoltaic technologies.[4−8] The current picture of organic photovoltaic operation focuses on free charge generation and subsequent recombination occurring through a manifold of weakly luminescent states formed at the interface between electron donor and acceptor phases (so-called "charge transfer" or "CT" states).[9−15]

From the analysis above, it follows that in an ideal organic photovoltaic material, 100% of photoexcitations should result in harvestable charges, and those photogenerated charges should recombine nongeminately via the CT state with 100% radiative efficiency, giving the blend a photoluminescence quantum efficiency (PLQE) of unity.

However, contrary to the relationship dictated by eq 1, for over two decades common practice in the field of organic photovoltaics has been to screen blend materials by evaluating their photoluminescence quenching efficiency (compared to the PLQE of their neat components) in contactless thin films, as the quenching of singlet exciton emission from the donor and acceptor components of the blend is taken to infer that a charge transfer event has taken place, based on the assumption that emission from the CT state is negligible.[16,17] While this method has been very successful for identifying blends that can efficiently generate charge, one might argue that it has delayed progress by pushing the field toward pairings of materials such as fullerene acceptors with intrinsically low PLQE.[18] In such materials, charges inevitably recombine through CT states with large losses to nonradiative recombination channels, as the vibrational modes that facilitate nonradiative recombination in the parent materials can couple with the CT states,[19] leading to large deficits in the maximum achievable open circuit voltage (V_{OC}).[9,20] Indeed, for polymer/fullerene solar cells with typical external radiative efficiency values in the range of 10^{-7}−10^{-4}%, this voltage loss due to nonradiative recombination is considerable (350−550 mV),[20−22] and indeed quite close to the excess "voltage deficit" these materials exhibit below the radiative limit as one would estimate from eq 1.[20−22] In this context, much work has focused on understanding and reducing nonradiative recombination pathways involving CT states at the interface between polymers and fullerenes.[19,20,23]

Recently, non-fullerene acceptors, both polymers and small molecules, have gained increasing attention, especially as their photovoltaic performance has matched and then exceeded that of polymer/fullerene blends.[24−30] Frequent advantages are cited in that they exhibit tunable and complementary absorption spectra that can improve light harvesting, and that they offer wider and more facile ranges of energy level tuning compared to fullerene acceptors. However, another compelling advantage of nonfullerene acceptors is the possibility that these materials may move the field out of the local minimum of radiative efficiency that resulted from optimization on photoluminescence quenching using polymer/fullerene pairings. Although worries persist that the high density of vibrational states that classically facilitate nonradiative recombination in large aromatic organic molecules[31] could lead to high rates of nonradiative recombination in an organic donor/acceptor system, it is encouraging to note that in the field of organic light emitting diodes similar intermolecular donor/acceptor exciplex states with very high photoluminescence quantum efficiency (20%) have been achieved,[32] whose properties can be tuned using a variety of different molecular engineering approaches.[33,34] Furthermore, recent advances in OPV over the last several years using nonfullerene acceptor molecules have led to devices with external electroluminescence quantum efficiencies (EQE_{EL}) on the order of 10^{-3}−10^{-2}%,[7,8] which are high by the standards of polymer/fullerene blends.[20,35] While the EQE_{EL} determines the nonradiative voltage loss of the solar cell itself,[2] the

DOI: 10.1021/jacs.8b05834
J. Am. Chem. Soc. 2018, 140, 9996−10008

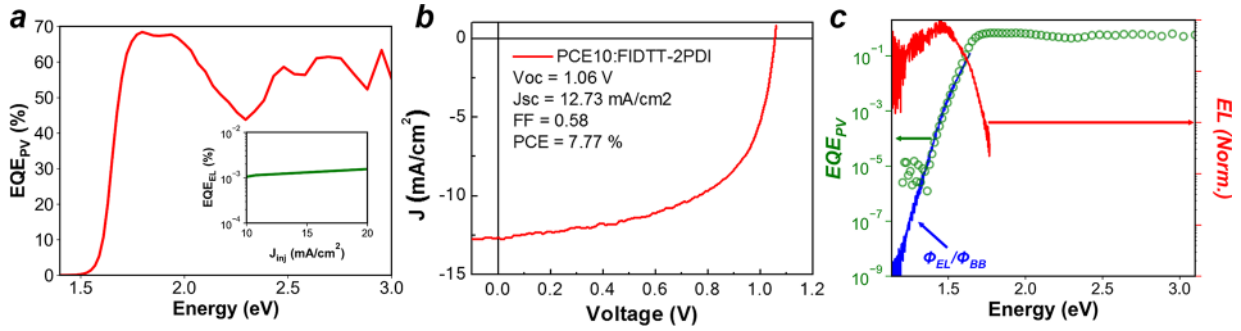

Figure 2. *a* EQE_{PV} spectrum of a 1:1 PCE10:FIDTT-2PDI device (*inset*: EQE_{EL} of a 1:1 PCE10:FIDTT-2PDI device displayed as a function of injected current density near 1 sun injection conditions). *b* Photovoltaic performance of a device based on 1:1 PCE10:FIDTT-2PDI blend measured under simulated AM1.5 illumination. *c* EQE_{PV} spectrum of 1:1 PCE10:FIDTT-2PDI measured using sensitive lock-in techniques to resolve the sub-bandgap absorption tail, along with the normalized electroluminescence spectrum. The blue line shows the EQE_{PV} tail recreated from the EL spectrum (ϕ_{EL}) and blackbody radiation spectrum (ϕ_{BB}), demonstrating the reciprocity relationship between the subgap EQE_{PV} and EL spectrum.

nonradiative recombination currents in a device can be influenced by parameters such as interface recombination at contacts[36,37] and leakage currents,[38] which are not strictly related to the intrinsic properties of the absorber material. Therefore, from a materials screening perspective, it is important to study OPV absorber materials that demonstrate the process of radiative recombination of photogenerated free charge.

Herein we study this question using a model blend system based on the donor polymer poly[[2,6′-4,8-di(5-ethylhexylthienyl)benzo[1,2-b;3,3-b] dithiophene] [3-fluoro-2[(2-ethylhexyl)carbonyl] thieno[3,4-*b*]thiophenediyl]] ("PCE10") and a pseudoplanar, small-molecule, nonfullerene acceptor consisting of an indacenodithieno[3,2-*b*]thiophene unit chemically fused with two perylene diimides ("FIDTT-2PDI"). This blend exhibits close to 80% photovoltaic internal quantum efficiency (IQE_{PV}) at short circuit, and exhibits relatively low V_{OC} loss (for organic photovoltaics) due to nonradiative recombination (ΔV_{nr}) of <300 mV (see below). Using time-resolved photoluminescence spectroscopy, we show that this blend exhibits *radiative* nongeminate recombination of photogenerated free charges out to microsecond time scales. Furthermore, we relate the low voltage losses to the microstructural and molecular properties of the blend and show that despite an apparently low driving force for charge transfer, the PCE10:FIDTT-2PDI system generates charge on early (picosecond) time scales. Together, these results demonstrate that the combined properties of efficient charge generation and photoluminescence due to nongeminate radiative recombination of charge are indeed possible in an efficient OPV blend, which demonstrates materials selection metrics that are needed to select OPV blends that will inherently achieve V_{OC}'s closer to the theoretical limits.

RESULTS AND DISCUSSION

Molecular Properties and Device Results. Figure 1a shows the molecular structure of the polymer donor and small molecule acceptor we use for these studies. This system comprises a blend of the widely used low band gap donor–acceptor alternating copolymer, PCE10, and a small molecule acceptor based on an acceptor–donor–acceptor (A–D–A) type structure which we refer to as FIDTT-2PDI. A fused-ring aromatic indacenodithieno[3,2-*b*]thiophene (IDTT) unit is used as a central donor aromatically fused with two electron withdrawing units of perylene diimide (PDI). The detailed synthetic route for FIDTT-2PDI is described in the Supporting Information (see SI Section S13). The IDTT core has been widely utilized[24] and its rigid ladder-type structure has the advantage of promoting $\pi-\pi$ stacking. However, the introduction of bulky alkyl side chains could lead to the dominance of intermolecular interactions occurring among the end groups.[28,39] With these factors in mind, we hypothesized that the aromatic fusing of IDTT and PDI unit could facilitate more crystalline solid state structures through the pseudoplanar configuration of a wide π-plane extended over the IDTT and PDI units. Figure 1b shows the UV–vis absorption spectra of thin films of FIDTT-2PDI, PCE10, and a 1:1 PCE10:FIDTT-2PDI blend. The FIDTT-2PDI acceptor has an optical absorption onset around 1.8 eV and strong absorption features in the range of 2.5–3.0 eV, which complements the absorption spectrum of the lower bandgap PCE10 and gives the PCE10:FIDTT-2PDI blend strong spectral absorption in the range of ∼1.6–3.5 eV.

Figure 2a shows the corresponding photovoltaic external quantum efficiency (EQE_{PV}) spectrum of a solar cell based on a 1:1 PCE10:FIDTT-2PDI blend (see Experimental Methods section for device structure). The device demonstrates a good incident photon to charge collection efficiency close to 70% at the absorption maximum of the PCE10:FIDTT-2PDI blend. Furthermore, the photovoltaic internal quantum efficiency (IQE_{PV}) is high at ∼70–80% across the full absorption spectrum of PCE10:FIDTT-2PDI (see SI Figure S3d and Section S3), which demonstrates that the conversion of absorbed photons to free charges, and their resulting collection is efficient in this system. From the EQE_{PV} spectrum, we can also calculate the short-circuit current (J_{SC}) of the device using the AM1.5 solar spectrum, which we find to be 13.2 mA/cm^2, in good agreement with the device performance measured under simulated AM1.5 illumination (Figure 2b).

Moving to examine nonradiative voltage losses, Figure 2a plots the external electroluminescence quantum efficiency (EQE_{EL}) as a function of injected current density (J_{inj}) near the J_{SC} for the solar cell operating under AM1.5 illumination. This current density is equivalent to the recombination current in the solar cell under 1 sun illumination and biased at the open-circuit voltage (V_{OC}).[9] Figure 2a shows that the EQE_{EL} under 1 sun equivalent injection conditions is approximately 1 × 10^{-3}%. Although well below values for GaAs and perovskite

DOI: 10.1021/jacs.8b05834
J. Am. Chem. Soc. 2018, 140, 9996–10008

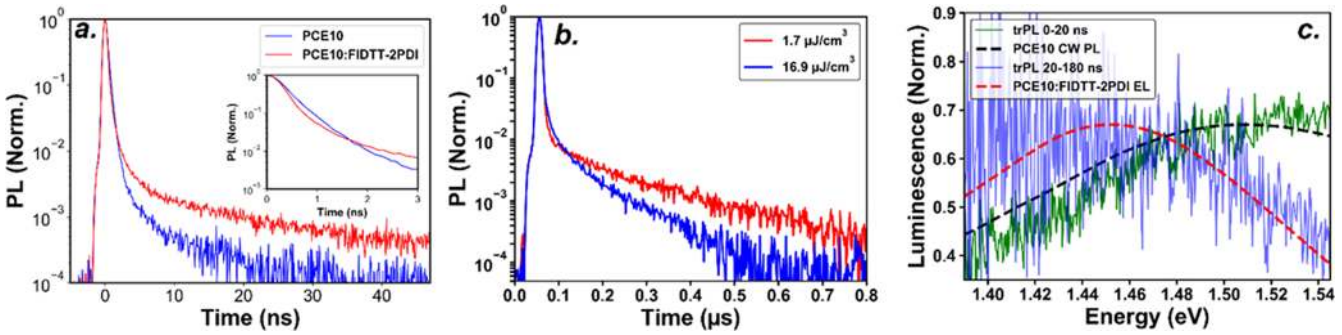

Figure 3. *a.* Time-resolved photoluminescence (PL) decays of neat PCE10 and 1:1 PCE10:FIDTT-2PDI following selective excitation of PCE10 at 735 nm (1.69 eV). The PCE10:FIDTT-2PDI blend exhibits a delayed luminescence tail extending beyond the 50 ns time window, (*inset*: early time (0−3 ns) time-resolved PL decay of PCE10 and PCE10:FIDTT-2PDI, showing fast initial quenching of the PCE10:FIDTT-2PDI luminescence). *b.* time-resolved PL decay of 1:1 PCE10:FIDTT-2PDI extended into the microsecond time window for two excitation fluences (1.7 μJ/cm^2/pulse and 17 μJ/cm^2/pulse), showing that the time-resolved PL tail exhibits fluence dependent kinetics characteristic of nonfirst order recombination. *c.* Time-integrated spectra from the time-resolved PL measurements showing that the emission redshifts during the long-time tail of the PL decay (20−180 ns) compared to the early time spectrum (0−20 ns). The steady-state PL spectrum of neat PCE10 and the EL spectrum of 1:1 PCE10:FIDTT-2PDI are shown overlaid on the 0−20 ns and 20−180s spectra, respectively. We note that the EL spectrum presented here is from the same data as Figure 2c but is smoothed by a low-pass filter (see SI Section S5 for details).

materials, this value is still among the highest values reported to date in an OPV device[7,8] and corresponds to a nonradiative voltage loss of only ∼292 meV which is among the lowest reported for an OPV device.[20] A complete understanding of the V_{OC} loss can be gained by analyzing the sub-band gap EQE_{PV} spectrum and electroluminescence (EL) spectrum in the framework of the reciprocity relations between the photogeneration and radiative recombination of free charge.[2,21,22,43] Following the approach taken by Nelson,[21] Kirchartz,[22] and Rau,[2] we use the electroluminescence spectrum measured at 1 sun equivalent injection to recreate and extend the sub-bandgap tail of the EQE_{PV} spectrum measured using photocurrent spectroscopy to calculate the nonideal radiative V_{OC} loss arising due to a nonstep-like band edge (absorption edge broadening).[21,22]

We first experimentally validate the reciprocity between the electroluminescence of PCE10:FIDTT-2PDI and the sub-bandgap EQE_{PV} spectrum by using the EL spectrum measured at 1 sun equivalent injection conditions (ϕ_{EL}) and the blackbody radiation spectrum at 295 K (ϕ_{BB}) to recreate the tail of the EQE_{PV} spectrum,[9,21,44] which is shown by the blue line labeled as ϕ_{EL}/ϕ_{BB} in Figure 2c and overlaid on the tail of the measured EQE_{PV} spectrum (see SI Section S2 for details on recreating the EQE_{PV} tail). Using the recreated EQE_{PV} spectrum extended down to low energies, we can then calculate the radiative saturation current J_0^{rad} to estimate the nonideal *radiative* V_{OC} loss (ΔV_{OC}^{rad}) using eqs 2 and 3:

$$J_{0,rad} = q\int_0^\infty EQE_{PV}(E)\phi_{BB}(E)\,dE \tag{2}$$

$$\Delta V_{OC}^{rad} = \frac{kT}{q}\ln\left(\frac{J_0^{SQ}}{J_0^{rad}}\right) \tag{3}$$

Using eqs 2 and 3 we calculate ΔV_{OC}^{rad} to be ∼68 mV, which is on the very low end of most OPV systems[21,22] and indicates a sharp absorption edge suggesting a low degree of disorder at the band edge. Considering a Shockley-Queisser limited V_{OC} of 1.381 V for a solar cell with a bandgap E_g^{PV} = 1.655 eV (see SI Section S1 for determination of E_g^{PV}), our measured values for ΔV_{OC}^{rad} (∼68 mV) and ΔV_{OC}^{nonrad} (292 mV) account quantitatively for the experimentally measured V_{OC} of 1.06 V (see SI Section S2 for full voltage loss analysis).

The collective device results demonstrate several important points about the PCE10:FIDTT-2PDI system: when incorporated in a solar cell, PCE10:FIDTT-2PDI shows not only efficient photoinduced free charge generation (IQE_{PV}), but also relatively efficient luminescence (EQE_{EL}) due to the recombination of injected free charge. Furthermore, by demonstrating the reciprocity between the EL and the EQE_{PV} spectra in Figure 2c, we conclude that the EL spectrum also represents the emission spectrum for the recombination of *photogenerated* free charge in PCE10:FIDTT-2PDI.[2] These properties make the PCE10:FIDTT-2PDI system well suited for studying the recombination of photogenerated free charge in photoluminescence, as we next turn to explore.

Photoluminescence from Radiative Nongeminate Charge Recombination. We study the radiative decay kinetics of pristine films of PCE10:FIDTT-2PDI using time-resolved photoluminescence spectroscopy by selectively exciting the PCE10 donor at 735 nm (1.69 eV). Importantly, this blend and excitation scheme allows us to monitor the decay kinetics of PCE10 polymer excitons and CT states *without any competing kinetic processes due to energy transfer* from FIDTT-2PDI to PCE10. In particular, we chose 735 nm as the excitation wavelength to selectively excite PCE10 because of the high (∼69%) IQE_{PV} of the PCE10:FIDTT-2PDI device at this wavelength compared to redder wavelengths in the IQE_{PV} spectrum, which maximizes the probability that charge generation would occur upon photoexcitation. In Figure 3a, we compare the time-resolved photoluminescence decay of neat PCE10 with PCE10:FIDTT-2PDI over a time window of 50 ns. At early times (∼0−2 ns), we observe a faster decay in PCE10:FIDTT-2PDI than neat PCE10, which indicates fast quenching of the initial excited state (singlet excitons on PCE10) due to charge transfer, as is typically seen in donor/acceptor OPV blends.[45,46] However, beyond 2 ns, we observe a long-lived delayed luminescence tail that extends out past the 50 ns time window in the PCE10:FIDTT-2PDI blend. *In contrast, we observe no such tail in the neat PCE10 film*, where the photoluminescence decays to the noise level at around 10 ns.

DOI: 10.1021/jacs.8b05834
J. Am. Chem. Soc. 2018, 140, 9996−10008

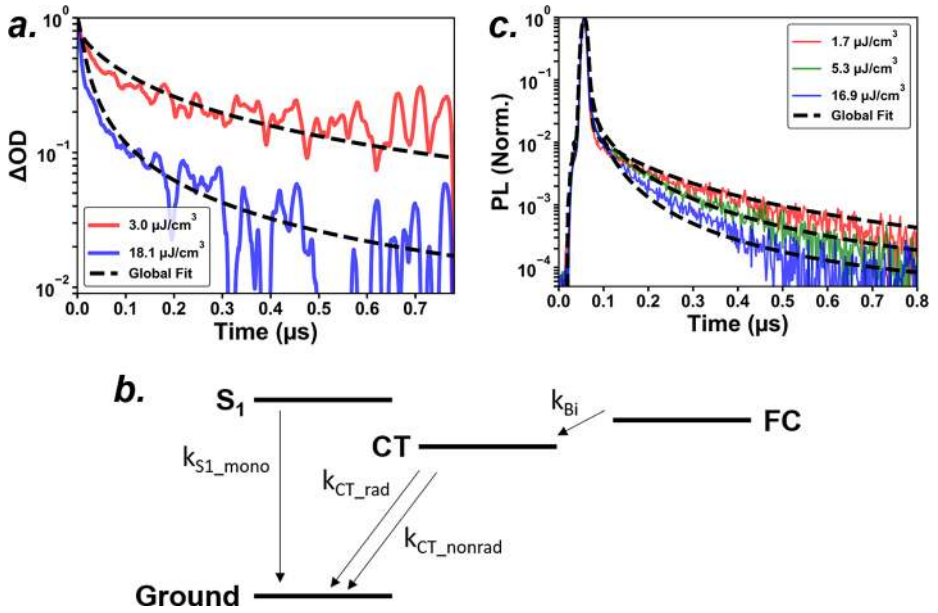

Figure 4. *a.* Fluence dependent photoinduced absorption decay of the polaron spectral feature from transient absorption (TA) spectroscopy. Results for the TA decay from the global fits to the TA and PL data sets based on the model in *b* are shown as black dashed lines. TA data is numerically smoothed for visual clarity, see SI section S8 for details. *b.* Schematic of the bimolecular decay model used to globally fit the photoluminescence (PL) and TA data. *c.* Fluence dependent time-resolved PL data along with the results for the PL decay based on the global fitting of the TA and PL data sets.

Delayed luminescence in neat polymer films has been widely studied, and is typically attributed to delayed fluorescence due to triplet−triplet annihilation[47−49] or phosphorescence[50,51] (the latter being observed only at cryogenic temperatures). On the contrary, delayed luminescence is less commonly reported in donor/acceptor blends: more often the photoluminescence of a donor/acceptor blend is strongly quenched due to charge transfer (followed by predominantly nonradiative decay), resulting in a faster observed photoluminescence decay in the blend than for either neat component.[52−54] There have been a few studies reporting long-time luminescence tails in organic donor/acceptor blends,[45,55−65] which have been explained almost exclusively as resulting from *geminate* recombination from a CT/exciplex state[45,55−59,62] or very rarely as radiative nongeminate charge recombination via a similar intermediate state.[60,61]

Here, we consider that the long luminescent tail that we observe in the PCE10:FIDTT-2PDI blends could arise from one of these possibilities, notably: (1) it could be the result of radiative nongeminate recombination of free charges; (2) it could result from slow geminate recombination of trapped CT states, or (3) it could result from the interplay of long-lived triplet states.

To test these possibilities further and distinguish whether the radiative recombination is due to a geminate or nongeminate process, we compare the photoluminescence decays at room temperature as a function of excitation fluence. Figure 3b shows the photoluminescence decay of the PCE10:FIDTT-2PDI blend extended out to a 1 μs time window, for two pump fluences that differ by an order of magnitude (1.7 μJ/cm^2/pulse and 17 μJ/cm^2/pulse). The decay kinetics of the delayed photoluminescence demonstrates a clear fluence-dependent increase in the decay rate with increasing pump fluence. A fluence-dependent increase in the apparent recombination rate is a clear indication of a nonfirst order process,[13,66] which suggests that the delayed photoluminescence does not arise from geminate CT recombination which should otherwise show first order kinetics, and can therefore be attributed to a nongeminate recombination process.

Figure 3c shows the time-integrated spectra from the time-resolved photoluminescence data in Figure 3b during the prompt (0−20 ns) and delayed (20−180 ns) time ranges. The prompt emission spectrum (0−20 ns) overlays well with the steady-state photoluminescence spectrum of PCE10 (black dashed line in Figure 3c), which is consistent with comparatively bright initial emission from PCE10 at early times before quenching occurs (as shown in the inset of Figure 3a). Although the signal-to-noise is low in the delayed photoluminescence spectrum (20−180 ns), we can see a clear redshift of the emission during the fluence-dependent emission tail, with the long-time spectrum showing good agreement with the electroluminescence spectrum of the PCE10:FIDTT-2PDI device (red dashed line in Figure 3c). As demonstrated earlier, the reciprocity between the electroluminescence spectrum and EQE_{PV} spectrum (Figure 2c) implies that the electroluminescence spectrum represents the emission spectrum for *photogenerated* free charges.[2] We thus consider the good spectral alignment between the electroluminescence and the time-delayed photoluminescence as evidence that the delayed photoluminescence in PCE10:FIDTT-2PDI arises from the nongeminate recombination of photogenerated charge carriers.

To further test our hypothesis that the delayed photoluminescence arises from the nongeminate recombination of charges, we use transient absorption (TA) spectroscopy to characterize the intensity-dependent excited state kinetics on the ns−μs time scale. Figure 4a shows the decay of the photoinduced absorption feature corresponding to the PCE10 polaron (see SI Section S10 for assignment of the TA feature and SI Section S8 for details about data processing). The polaron absorption measured via TA exhibits fluence-depend-

DOI: 10.1021/jacs.8b05834
J. Am. Chem. Soc. 2018, 140, 9996−10008

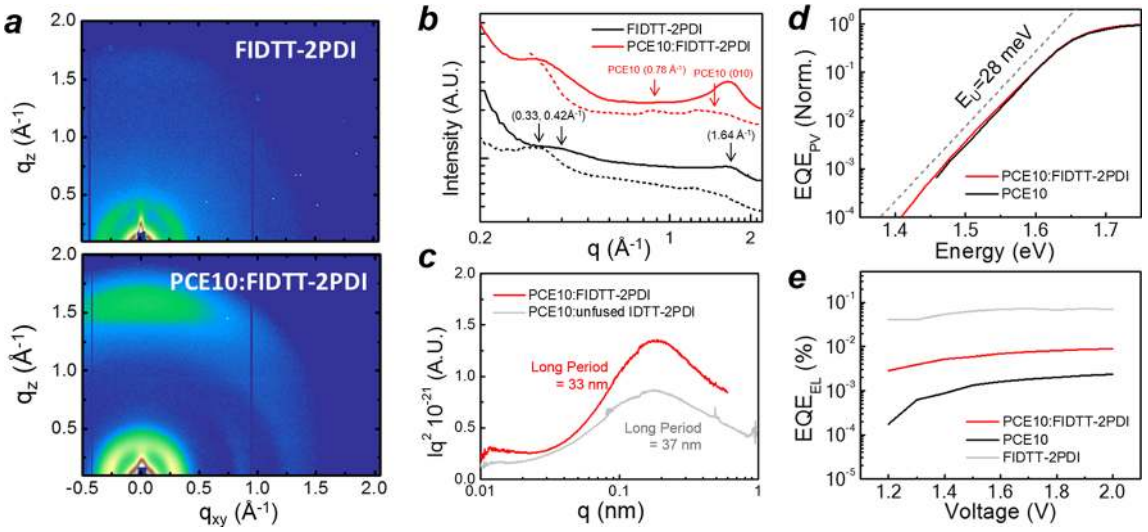

Figure 5. *a* 2D grazing-incidence X-ray diffraction patterns of neat and blend films at optimized conditions and *b* their 1D line-cuts in out-of-plane (solid lines) and in-plane (dotted lines) directions. *c* Thickness normalized and Lorentz-corrected resonant soft X-ray scattering profiles acquired at 283.4 eV. The unfused version of FIDTT-2PDI is included for comparison, which has similar long periods with lower domain purity. *d* Subgap EQE_{PV} spectra and *e*. EQE_{EL} with respect to applied voltage for neat and blend films. Dotted lines in *d* demonstrates an Urbach energy of 28 meV.

ent kinetics on the same time scale as the delayed photoluminescence when excited at the same wavelength (735 nm) with comparable pump fluences (3.0 $\mu J/cm^2$/pulse and 18.1 $\mu J/cm^2$/pulse). Taken together, this data provides further evidence for the nongeminate recombination of photogenerated charge to explain the long photoluminescence tail.

To compare the TA kinetics to the delayed photoluminescence in a more quantitative fashion, we use a simplified model for bimolecular recombination resulting in radiative and nonradiative decay to perform global fits of both the time-resolved photoluminescence data and the transient absorption data. In this approach, we fit all of the fluence-dependent TA and time-resolved photoluminescence data sets *simultaneously* using a common set of parameters using the bimolecular recombination model as shown schematically in Figure 4b.

Briefly, we model the time-dependent free-carrier population (FC), PCE10 exciton population (S_1), and CT state population (CT), using a set of coupled ordinary differential equations (see SI Section S4 for more details about the model and simulation parameters). As shown in Figure 4b, in this model the luminescent recombination of charge in PCE10:-FIDTT-2PDI occurs via a CT state, which is consistent with the observation of a red-shifted electroluminescence spectrum in the PCE10:FIDTT-2PDI blend compared to either of the neat components (see SI Figure S5b).

Figure 4a, c shows the results of the global fits to the TA and time-resolved photoluminescence data. The fits converge with a bimolecular charge recombination rate of $k_{bi} = 2.23 \times 10^{-11}$ cm^3/s, which is of similar order of magnitude for bimolecular charge recombination rates measured in a wide range of OPV blends.[67] Furthermore, by allowing the radiative and non-radiative recombination rates of the CT state to vary in the fit, we extract a monoexponential lifetime $\tau_{CT_{mono}}$ for the CT state of ~3.97 ns (where $\tau_{CT_{mono}} = 1/(k_{CT_{rad}} + k_{CT_{nonrad}})$) which is in good agreement with monoexponential CT lifetimes reported in the literature,[57,63,64] and a PLQE for the CT state of 1.36×10^{-2}%, which is consistent with the value that we estimate for the CT PLQE based on steady state photoluminescence measurements (see SI Section S7).

We point out that our model only requires the basic assumption of second order kinetics for nongeminate charge recombination (as opposed to many other models in the literature that require empirical reaction orders to fit nongeminate kinetics in OPV systems[68,69]), and based on this simplified model we consider the global fits to the TA and photoluminescence data to be very good. We consider that the agreement between the fit to the polaron decay in the TA data and the time-resolved photoluminescence data based on a set of common reasonable parameters, along with the agreement between the delayed photoluminescence spectrum and the EL spectrum to be strong evidence in favor of the origin of the delayed photoluminescence in PCE10:FIDTT-2PDI resulting from the radiative nongeminate recombination of free charge.

Returning to the possibility that the long nongeminate photoluminescence tail could arise from the dynamics of triplet states,[47−49,59] we note that Gelinas et al.[59] observed fluence-dependent delayed luminescence in F8BT:PFB polymer/polymer blends at low temperature (10 K), which they attributed to triplet−triplet annihilation. We believe that triplet−triplet annihilation is an unlikely origin for the delayed photoluminescence observed in our system based on (1) the stronger delayed photoluminescence tail in the blend compared to the PCE10 which would be inconsistent with the formation of triplets via intersystem crossing from the PCE10 singlet; and (2), the radiative lifetime obtained for the emissive state in the delayed photoluminescence from our global fits to the data in Figure 4a, c, which is inconsistent with the expected radiative lifetime if the emissive state were due to triplet−triplet up-conversion, regardless of the origin of triplet formation (see SI Section S9 for a detailed discussion).

We note that Keivanidis et al.[60,61] have also observed delayed luminescence in polymer/small molecule blends of F8BT:PDI and related systems, which they also attributed to the nongeminate recombination of charge via exciplex emission. However, in contrast to the PCE10:FIDTT-2PDI system studied here, solar cells based on F8BT:PDI systems

DOI: 10.1021/jacs.8b05834
J. Am. Chem. Soc. 2018, 140, 9996−10008

generally exhibit low charge generation efficiency (EQE_{PV} not exceeding ~17%) and poor device performance (PCE < 0.1%),[70] raising the possibility that efficient radiative recombination of nongeminate polarons and efficient charge separation/extraction might be mutually exclusive processes. Importantly, we point out that the PCE10:FIDTT-2PDI system we study here appears to generate photocurrent efficiently (EQE_{PV} approaching 70%), *and* exhibits photoluminescence due to the radiative nongeminate recombination of charge. Given that efficient charge generation and radiative nongeminate recombination of photogenerated charge are basic requirements needed to approach theoretical efficiency limits for solar cells, we believe that finding other organic donor/acceptor systems that exhibit maximum efficiencies for these processes simultaneously will be an important step toward selecting materials to realize higher V_{OC} and ultimately the highest power conversion efficiencies. To further understand the V_{OC} losses in our system, we next turn to examine the possible molecular and morphological origins related to the low V_{OC} losses in the PCE10:FIDTT-2PDI blend.

Molecular and Microstructural Aspects of Low Voltage Loss. To gain further insight into the voltage losses of the PCE10:FIDTT-2PDI blend with respect to the molecular properties of the FIDTT-2PDI acceptor, we investigate the microstructure of both neat acceptor and blend films, and the physical structure of donor/acceptor interfaces, using 2D grazing-incidence wide-angle X-ray scattering (2D GIWAXS) and resonant soft X-ray scattering (RSoXS).[71,72] Figure 5a depicts the 2D GIWAXS patterns of neat FIDTT-2PDI and the PCE10:FIDTT-2PDI blend films, and Figure 5b shows their 1D profiles in both the out-of-plane and in-plane directions. The neat FIDTT-2PDI film exhibits characteristic diffraction peaks at 0.33 $Å^{-1}$ (in-plane), 0.42 $Å^{-1}$ (out-of-plane) and 1.64 $Å^{-1}$ (out-of-plane). The *d*-spacings of these peaks of FIDTT-2PDI are slightly different from those of the lamellar stacking (0.29 $Å^{-1}$) and $\pi-\pi$ stacking (1.59 $Å^{-1}$) of PCE10, respectively. Interestingly, both crystal diffraction peaks of FIDTT-2PDI are more pronounced in the blend, along with the formation of preferential face-on orientation of PCE10 as exhibited by the pronounced (010) peaks in the out-of-plane direction. This level of molecular order suggests the molecules in the bulk heterojunction have formed self-aggregated domains. However, due to the strong intermolecular interactions, it is also possible that unfavorable domains (larger than the exciton diffusion length) could form, although in such cases one would expect a decrease in device performance.

We next probe the domain characteristics of the PCE10:FIDTT-2PDI blend with resonant soft X-ray scattering (RSoXS). Figure 5c shows the Lorentz-corrected RSoXS profile of the blend acquired at 283.4 eV, where the material contrast is maximum. The average domain purity can be quantified by a parameter called the mean-square composition variance, which scales with the area integration of RSoXS profile normalized by film thickness and materials contrast.[71] By comparing the blend morphology of FIDTT-2PDI and its unfused version, we find that the mean-square variance of the PCE10:FIDTT-2PDI system is ~1.5 times of that of its unfused counterpart. Additionally, the profile in Figure 5c is well fitted to a single log-normal distribution. Assuming the samples are globally isotropic in 3 dimensions, the length scale of domains can be estimated by 2π over q of the scattering peak. The long period extracted from the profile of the PCE10:FIDTT-2PDI film is estimated to be 33 nm, which agrees well with the size scale measured in transmission electron microscopy showing well-distributed crystal domains (see SI Figure S12). Consequently, these results indicate that crystalline domains maintaining reasonable long periods of approximately 33 nm and relatively higher domain purity are formed in the PCE10:FIDTT-2PDI blend.

Importantly, the observation of high domain purity and ordered packing is also well-correlated with the low degree of disorder-induced broadening of the EQE_{PV} tails in the PCE10:FIDTT-2PDI blend. Figure 5d compares the subgap EQE spectra of neat PCE10 and PCE10:FIDTT-2PDI blend devices. As compared to the EQE_{PV} of neat PCE10, it is clear that the blend film exhibits only a subtle broadening of the band edge with an Urbach energy as low as 28 meV, which we attribute to a narrow density of subgap states in the PCE10:FIDTT-2PDI blend.[15,73] Furthermore, a comparison of the EL spectra between neat PCE10 and the PCE10:FIDTT-2PDI blend (SI Figure S5b) shows that the EL emission peak in the blend is only ~45 meV red-shifted compared to that of neat PCE10. On the basis of these observations we hypothesize that charge recombination occurs via a narrow distribution of high energy charge transfer states.

We note that, in the common theory used to analyze CT state absorption and emission, the peak of the electroluminescence spectrum occurs at an energy equal to ($E_{CT} - \lambda$), where E_{CT} is the CT state energy and λ is the reorganization energy, the latter is related to the geometric relaxation of the molecule following absorption or emission between the ground and excited CT complex.[43] On the basis of the position of the EL peak (1.45 eV) in the PCE10:FIDTT-2PDI blend, and considering that the upper limit of E_{CT} should not exceed E_g^{PV} = 1.655 eV (the S_1 energy of PCE10), we can estimate an upper limit on λ of ~0.2 eV. We take this value for λ to be a conservative upper limit since the ~45 meV red-shifted electroluminescence spectrum suggests that E_{CT} is several 10s of meV lower than E_g^{PV}. Indeed, based on fitting the EQE_{PV} and EL spectra to the model derived by Vandewal and co-workers[43] where the value of λ is further constrained to fit the width of the EL spectrum and EQE_{PV} tail, we find that λ is closer to 0.15 eV (see SI Section S10 and Figure S10), which falls on the very low end of values for λ that have been reported for polymer/small molecule acceptor blends ($\lambda \approx$ 0.1−0.4 eV).[43,74,75] Both the crystallographic results and CT state analysis suggest a microscopic origin—specifically low interfacial disorder and a small reorganization energy—for the low nonideal radiative voltage loss (ΔV_{OC}^{rad}) calculated based on the EL and EQE_{PV} reciprocity analysis in Figure 2e above.

In addition to affecting the nonideal radiative voltage loss, recent work has highlighted the role of both high E_{CT} and small λ in mitigating inherent nonradiative recombination from the excited state CT complex, originating from the skeletal chemical bonding.[19,20] We can speculate that the small λ for the CT transition may be associated with the structural rigidity of the FIDTT-2PDI acceptor due to its aromatically fused structure, which may be responsible for helping mitigate nonradiative recombination from the CT state.[19,76] Most obviously, the suppression of nonradiative pathways in films of neat FIDTT-2PDI is evident from its PLQE of 5%, which exceeds that of neat PCE10 (PLQE = 3%, see SI Section S6 for details about PLQE measurements of the neat materials) and is orders of magnitude higher than PLQE values measured for fullerenes.[18] In addition, the EQE_{EL} of neat FIDTT-2PDI

DOI: 10.1021/jacs.8b05834
J. Am. Chem. Soc. 2018, 140, 9996−10008

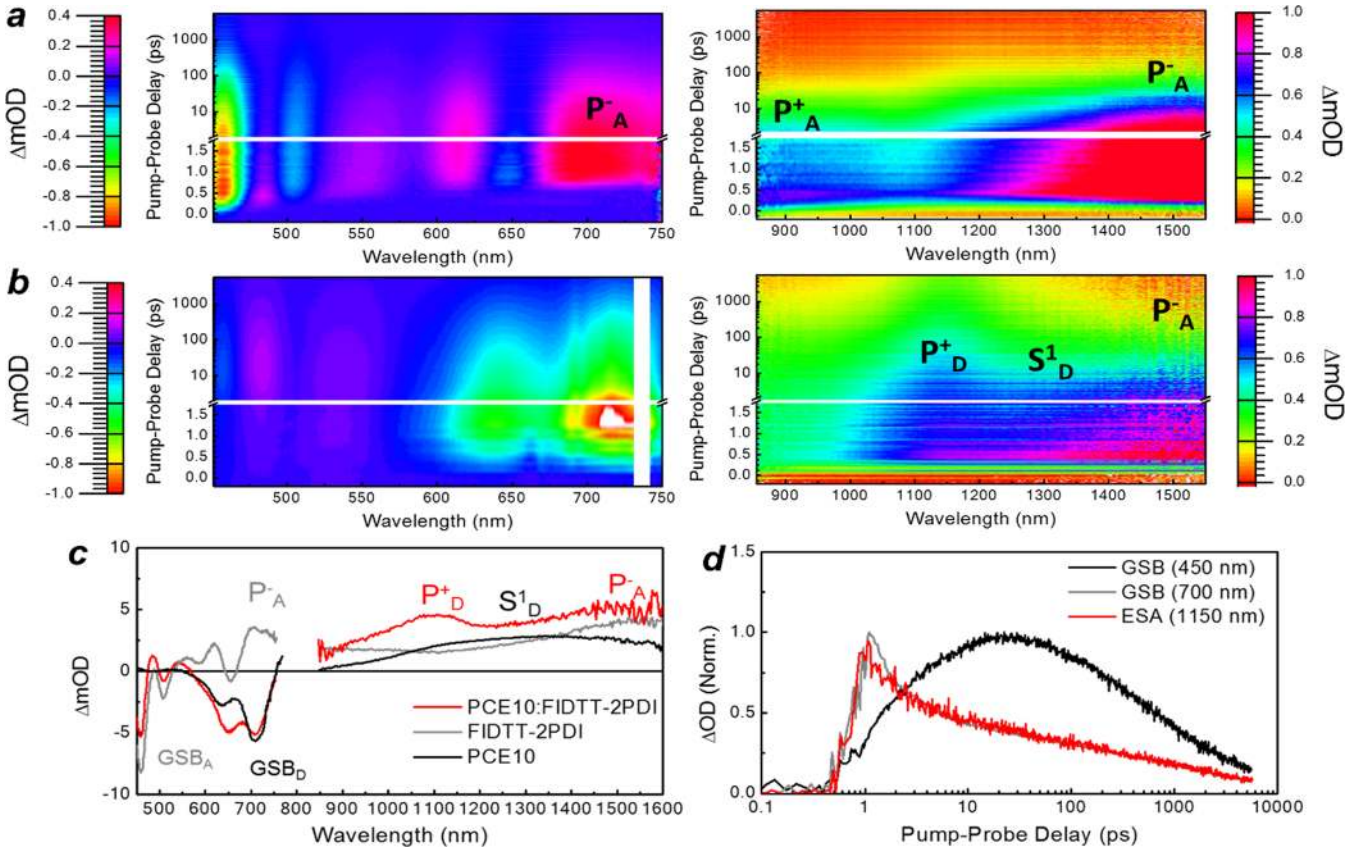

Figure 6. Pseudocolor plot broadband transient absorption spectra of *a* neat FIDTT-2PDI films and *b* PCE10:FIDTT-2PDI blend films at processed optimized conditions. *c* Initial (2 ps) spectra of photoinduced absorption and bleaching for neat and blend materials excited at 500 nm pump wavelength. The spectral features are labeled by the assignments. *d* Kinetic traces of the spectral features in *b*. The pseudocolor plots are based on 0.03 isosurface on normalized scale. The FIDTT-2PDI signals are normalized to ΔmOD of −6 and 8 for visible and near IR range, respectively. The blend signals are normalized to ΔmOD of −20 and 6.5 for visible and near IR range, respectively.

(Figure 5e) reaches efficiencies up to 0.1%, which is comparable to the EQE_{EL} typically measured for crystalline silicon solar cells[21] and for another common acceptor molecule with a rigid IDTT core, ITIC.[75] Therefore, we postulate that the inherent properties of the neat FIDTT-2PDI molecule that allow it to achieve high radiative efficiency on its own may be helping to suppress nonradiative decay pathways via the CT state in the PCE10:FIDTT-2PDI blend.

Ultrafast Charge Transfer Kinetics. On the basis of the above analysis we hypothesized that charge recombination occurs via a narrow distribution of high-energy CT states, in a highly crystalline, well ordered material. The energetic offset between the CT state energy and the excited state of the donor or acceptor,[8] and the energetic gradient between carriers in ordered and disordered regions of the material,[77−81] have both been posited as primary driving forces for charge separation. However, since the PCE10:FIDTT-2PDI blend minimizes both of these potential driving forces, it is interesting to consider the charge transfer dynamics in this blend given its relatively high IQE_{PV} values.

To understand the kinetics of the initial charge generation process, we performed femtosecond transient absorption spectroscopy. Figure 6a, b shows pseudocolor plots of the evolution of the excited state absorption (ESA) and ground state bleach (GSB) features. Due to the energetic separation of their absorption onsets (Figure 1c), FIDTT-2PDI and PCE10 exhibit distinct ground state bleach spectra. On the basis of preliminary assignments of the spectral features (see Figure 6c and SI Section S11), we attribute the ESA features at 700 nm, 900 nm, and a broad feature centered at 1500 nm correspond to the charged species of FIDTT-2PDI, while we assign the features at 1150 and 1400 nm to the polaron and singlet state of PCE10,[82] respectively. For measurements on the blend films, we selectively excited PCE10 using 735 nm excitation at a fluence of 2.7 $\mu J/cm^2$/pulse, which corresponds to excitation densities on the order of $\sim 10^{17}/cm^3$. As noted earlier, the selective excitation of PCE10 below the band edge of FIDTT-2PDI simplifies interpretation of the data by allowing us to rule out effects due to energy transfer from FIDTT-2PDI to PCE10.

The green trace in Figure 6d shows the combined kinetics of the PCE10 polaron and the tail of broad PCE10 singlet ESA features. The initial fast decay of the ESA at 1150 nm results from singlet decay (quenched lifetime of 3 ps), which is then dominated by decay of the polaron feature (see SI Section S11 and Figure S11.3 for global analysis). The invariance of the peak position as well as its fluence dependence (see SI Section S11 and Figure S11.3) indicate that the polaronic feature becomes charge separated state rather than remaining in the initial geminate polaron pair.[83,84] Therefore, we deduce that the majority of charges are separated faster than the geminate decay through CT states (τ_{CT} = 3.97 ns based on the modeling of the delayed photoluminescence, see SI Section S4). The excited state kinetics in neat PCE10 are included in SI Section S11 for comparison. Interestingly, the GSB of FIDTT-2PDI shows an obvious signature of charge transfer, with a

DOI: 10.1021/jacs.8b05834
J. Am. Chem. Soc. 2018, 140, 9996−10008

continuously growing signal until 13 ps. This further demonstrates that the population of excited states in the acceptor domain is dominated by the transfer of charges from PCE10 without any initial population by direct excitation, where the GSB rise time is the result of a balance between charge generation and recombination.

These results demonstrate that, despite an apparently low energetic driving force for charge transfer, efficient charge transfer occurs on picosecond time scales in the PCE10:FIDTT-2PDI blend. This is consistent with time scales for charge transfer observed in other efficient polymer/nonfullerene systems,[85,86] although we remark that it is slower than the ultrafast (subpicosecond) charge transfer time scales observed in polymer blends with fullerene and other nonfullerene acceptors.[14,82] Together with the microstructural studies discussed above, these data support a picture where favorable delocalization of CT states through the high local crystallinity aids in the charge generation process, which agrees with recent studies that demonstrate the delocalization of charges away from the interface plays a key role in dissociating charge transfer states.[11,64,84,87−90]

CONCLUSIONS

We have studied the voltage losses and nanosecond-to-microsecond scale charge recombination processes in a nonfullerene acceptor blend of the common donor polymer PCE10 and a nonfullerene acceptor FIDTT-2PDI, comprising an IDTT core based A−D−A type molecule with a fully fused pseudo planar structure. In optimized blends, these materials exhibit good power conversion efficiencies over 7.5% with relatively high EQE_{PV} (70% max) and low V_{OC} loss compared to the Shockley-Queisser limit. This low voltage loss can be attributed to both a low nonideal radiative loss (∼68 mV) due to a sharp band edge, and a relatively low nonradiative loss (292 mV) due to an EQE_{EL} that reaches $\sim 1 \times 10^{-3}$%. Importantly, this blend shows a long-lived tail out to ∼1 μs in the transient photoluminescence decay. From the analysis of the intensity-dependent photoluminescence and intensity-dependent transient absorption kinetics, we conclude that this long emission tail results from the radiative nongeminate recombination of photogenerated free charge carriers.

We propose that the low nonideal radiative voltage loss in PCE10:FIDTT-2PDI can be understood based on a high degree of interfacial crystallographic order in the blend due to favorable intermolecular interactions promoted by the extended π-conjugated structure of FIDTT-2PDI, which results in a small Urbach energy at the band edge (∼28 meV) that we propose reflects a narrow distribution of high energy subgap CT states. We also found that the radiative efficiency of the FIDTT-2PDI molecule itself is good, exhibiting a PLQE of 5% and EQE_{EL} of 0.1%. On the basis of these observations, we speculate that the low nonradiative voltage loss in the PCE10:FIDTT-2PDI blend is related to the molecular properties of FIDTT-2PDI itself. Recent work has emphasized the relationship between the radiative efficiency of the donor/acceptor CT state and the low frequency intramolecular vibrational modes of the parent molecules that can induce structural reorganization which facilitates nonradiative decay to the ground state via skeletal vibrations.[19,76] We therefore hypothesize that the fully fused rigid structure of FIDTT-2PDI may be responsible for the good radiative properties of the molecule itself and the radiative efficiency of the PCE10:FIDTT-2PDI blend, while the narrowing of the CT density of states due to the highly crystalline interfaces may also help to suppress nonradiative recombination from tail sites with lower CT energies.[20]

Most importantly, our observation of photoluminescence due to nongeminate charge recombination in this system has important implications on the selection and evaluation of donor/acceptor pairs for future OPV blends. Photoluminescence due to the recombination of photogenerated free charge is a basic prerequisite for achieving maximum theoretical open circuit voltages in solar cells and is frequently used as a screening metric for high V_{OC} in crystalline inorganic materials that undergo band-to-band radiative recombination.[91,92] However, photoluminescence due to nongeminate charge recombination has rarely been characterized in OPV blends based on the assumption that efficient generation of charge will be correlated with recombination via pathways that are predominantly nonradiative. In this sense, we propose that for the new generation of donor/acceptor systems based on more highly emissive polymer/nonfullerene acceptor blends, a new materials screening metric that is based on the efficiency of nongeminate free charge photoluminescence is necessary to push researchers in the path toward selecting blends that will maximize V_{OC}. To this end, selecting materials based on the photoluminescence quantum efficiency of the individual donor and acceptor parent molecules may help select blends with inherently more highly luminescent CT states, ultimately enhancing the radiative efficiency of free charge recombination. In addition, comparing photoluminescence due to nongeminate charge recombination in isolated films versus completed devices at V_{OC} may be able to help reveal information about nonradiative charge recombination occurring at contacts. As pointed out by Keivanidis et al.,[61] in a blend where recombination of free charge occurs radiatively, the absolute intensity of photoluminescence due to free charge recombination will also scale with the charge generation efficiency. Therefore, we believe that ultimately, screening organic photovoltaic blends based on both the efficiency and intensity of photoluminescence due to nongeminate recombination of charge will help select blends that can achieve the highest power conversion efficiencies.

EXPERIMENTAL SECTION

Device and Sample Fabrication. Devices were fabricated using patterned ITO/glass substrates (Thin Film Devices, Inc. Fifteen Ω sq-1), while samples for spectroscopy were prepared on glass microscope slides, which were cleaned by sonication consecutively in detergent solution, DI-water, acetone, and isopropanol, followed by UV−O_3 treatment (Jelight 144AX). For devices, a zinc acetate dihydrate (1 g) solution dissolved in 2-methoxy ethanol (10 mL) and ethanolamine (280 μL) was spin-coated on the cleaned substrates at 4000 rpm and sintered at 220 °C for 1 h in air resulting in a 30 nm thick ZnO film. The PCE10:FIDTT-2PDI solutions were prepared by dissolving a 1:1 wt % ratio of PCE10 (1-Material, Inc.) and FIDTT-2PDI to a total concentration of 20 mg/mL in anhydrous 1,2-dichlorobenzene with 3% by volume 1-chloronapthalene. Neat polymer solutions were prepared by dissolving 10 mg/mL PCE10 in anhydrous 1,2-dichlorobenzene. Neat acceptor solutions were prepared by dissolving 10 mg/mL FIDTT-2PDI in anhydrous chloroform. Solutions in 1,2-dichlorobenzene were blended at 90−100 °C for 12 h inside of a N_2 glovebox, while solutions in chloroform were stirred for several hours inside the glovebox. PCE10:FIDTT-2PDI blend and neat films were prepared inside of a N_2 glovebox by spin-coating the solutions at 1600−1800 rpm for 2 min on the ZnO/ITO/glass substrates for devices and on glass substrates for spectroscopy. For devices, 6 nm of MoO_X and 120 nm of Ag were thermally evaporated (<1e-6 Torr,

DOI: 10.1021/jacs.8b05834
J. Am. Chem. Soc. 2018, 140, 9996−10008

Angstrom Engineering EvoVAC) through a patterned shadow mask to define the electrode pattern. The electrode area for devices defined by the overlap between the MoOx/Ag and ITO electrodes was approximately 0.06 cm^2. For spectroscopy, the films on glass were encapsulated inside of a N_2 glovebox using epoxy to seal a glass-to-glass bond between the perimeter of the sample substrate and a glass cover slide.

Photovoltaic Performance, Quantum Efficiency, and Optical Absorption Spectroscopy. Photovoltaic performance was evaluated by measuring the current−voltage characteristics (Keithley 2400) of the PCE10:FIDTT-2PDI solar cell under simulated AM1.5G illumination using a Class A solar simulator (Solar Light Co. 16S-300) inside of a N_2 glovebox. A calibrated reference silicon photodiode was used to calibrate the incident light intensity. Photovoltaic external quantum efficiency (EQE_{PV}) was measured using a custom built split-beam spectrometer with the device held under dynamic vacuum (<50 mTorr) inside a custom-built vacuum chamber with fused silica windows for optical spectroscopy. Light from a tungsten-halogen lamp (Horiba Scientific PowerArc) was spectrally filtered using a monochromator equipped with an order-sorting filter (Princeton Instruments SP-2150) and chopped at a frequency of 220 Hz (Stanford Research Systems SR540). Long pass filters with cut-on wavelengths at 750, 800, and 850 nm were additionally used to filter any scattered light from the monochromator. The light was split using a fused silica optic so that a small fraction of the beam was focused onto a Si photodiode used to monitor intensity fluctuations from the incident light, while the remainder of the light focused onto a pixel of the device through a small area aperture mask. The photocurrent signal from the device was amplified with a transimpedance amplifier (Stanford Research Systems SR570) with no input bias, and the signal was demodulated by a lock-in amplifier (Stanford Research Systems SR830). The photocurrent from a calibrated Si photodiode (OSI Optoelectronics) was then measured at the sample position through the same aperture mask to measure the incident power and calculate EQE_{PV}. Differences in lamp intensity between the two measurements were corrected using the signal recorded by the photodiode receiving the split-beam intensity. To calculate the internal quantum efficiency (IQE_{PV}) spectra, the complex refractive index spectra (n and k) of all layers in the device were determined using spectroscopic ellipsometry (J.A. Woollam Co. M-2000, see SI Section S3 for details) and the fraction of absorbed light in the active layer was calculated using transfer-matrix modeling. UV−vis absorbance spectra were measured on encapsulated samples using a diode array UV−vis spectrometer (Agilent 8453). A sample consisting of two pieces of glass epoxied together around the perimeter was used as a blank for UV−vis absorbance.

Electroluminescence and Steady State Photoluminescence Spectroscopy. Electroluminescence spectra were measured driving the device with a DC voltage (Keithley 2400) while held under dynamic vacuum (<50 mTorr) inside a custom-built vacuum chamber with fused silica windows for optical spectroscopy. The device was aligned to the focal point of a custom-built spectrometer based on a f/3.9 spectrograph (Princeton Instruments SP-2300, slit width = 200 μm) and a f/4 lens system to collect the luminescence. The spectra were recorded with a LN_2 cooled CCD detector (Princeton Instruments Spec-10) and were corrected for the spectral response of the system using a calibrated white light source (Ocean Optics HL-3P-CAL-EXT). Electroluminescence quantum efficiency (EQE_{EL}) was measured inside of a N_2 glovebox using a custom built setup consisting of a large area calibrated Si photodiode (Hamamatsu S3204−08), and two source-meters (Keithley 2400 and Keithley 237) used to simultaneously drive the device and measure photocurrent due to the photon flux indecent on the Si photodiode. Following standard procedures for OLED measurements,[93] the device was placed nearly flat on the photodiode with waveguided emission effectively blocked by the sample holder, while the small device area (~0.06 cm^2) relative to the detector area (~1 cm^2) ensured that the measurement was close to the condition of underfilling the detector. Steady-state photoluminescence spectroscopy was measured using a custom built set up consisting of a set of f/3 achromatic lenses used to collect and focus sample luminescence into a fiber optic cable (NA = 0.22) coupled to a compact CCD spectrometer (Ocean Optics, USB 2000+). The sample was excited with either a focused 730 nm diode laser (Thorlabs HL7302MG) or a collimated 532 nm DPSS laser (CrystaLaser). Photoluminescence quantum efficiency (PLQE) of neat FIDTT-2PDI and PCE10 thin films on glass was measured inside of a N_2 glovebox using a modified set up based around a Hamamatsu C9920−02 integrating sphere system. Briefly, a 532 nm DPSS laser (CrystaLaser) was fiber coupled into the integrating sphere, and the laser intensity as well as sample luminescence were simultaneously measured using a CCD spectrometer (Hamamatsu C10027) that was fiber coupled to the output port of the integrating sphere. Three measurements (sample in laser path, sample out of laser path, and sample removed from sphere) were made and the PLQE was calculated using the method of de Mello and co-workers.[94]

Time-Resolved Photoluminescence Spectroscopy. Time-resolved photoluminescence spectra were measured using a streak camera with excitation from an ultrafast tunable laser source. In brief, the fundamental output of a Ti:sapphire amplifier (Coherent, Inc. Libra-HE, 4.0 mJ, 1 kHz, 50 fs) was used to pump an optical parametric amplifier (Coherent, Inc./Light Conversion OPerA Solo) which was used to tune the laser excitation wavelength to 735 nm. Appropriate long-pass and band-pass filters were used after the OPA to ensure a clean laser spectrum, and the beam profile was measured prior to each experiment to quantify the excitation area (Thorlabs BC106N−UV). Luminescence from the sample was collected using a set of f/4 lenses which focused the light into a f/3.9 spectrograph (Princeton Instruments SP-2150, entrance slit width = 200 μm) coupled to a streak camera (Hammamatsu C10910, slow-sweep unit M10913−01). The streak camera was operated in photon-counting mode using maximum gain, and signal levels <5% above the photon counting threshold were maintained using neutral density filters in front of the detector to ensure single photon counting statistics. The time-resolved PL spectra were corrected for the spectral response of the system by measuring the spectrum of a calibrated white light source (Ocean Optics HL-3P-CAL-EXT) on the streak camera operated in focus mode. Appropriate subtraction of dark spectra were accounted for when correcting the white light and time-resolved PL spectra. All spectra were additionally corrected for the transmittance of a long-pass (800 nm) filter and any neutral density filters used on the detector. The IRF of the streak camera was measured using a ground glass slide to scatter part of the laser excitation into the detector with the signal attenuated by nonfluorescing neutral density filters.

Transient Absorption Spectroscopy. Transient absorption spectra were measured using a Helios/EOS spectrometer (Ultrafast Systems) built around the same laser amplifier used for time-resolved photoluminescence. In brief, the fundamental output of the Ti:sapphire amplifier (Coherent, Inc. Libra-HE, 4.0 mJ, 1 kHz, 50 fs) was split into two beamlines by an 80/20 beam splitter. Part of the fundamental beam was used to pump an optical parametric amplifier (Coherent, Inc./Light Conversion OPerA Solo) which was used to tune the pump laser wavelength to 735 nm. For femtosecond transient absorption spectra, the other part of the fundamental beam was used to generate a white continuum probe using CaF_2 or sapphire plates. The delay between pump and probe pulses was controlled using a mechanical delay stage. For nanosecond transient absorption spectra, the white light continuum probe was generated using a supercontinuum pulsed light source which is electronically delayed relative to the pump. The ΔOD spectra were collected using fiber-coupled silicon CMOS and InGaAs array detectors while chopping the pump light at 500 Hz (for ultrafast measurements) or electronically modulating the probe at 2 kHz (for nanosecond measurements) to alternate collection of "pump-on" vs "pump-off" spectra. Appropriate long-pass and band-pass filters were used to ensure a clean pump laser spectrum and the beam area was quantified using a beam profiler (Thorlabs BC106N−UV). The spectra were processed by subtracting an average of 20 background noise spectra before time zero, performing chirp-correction and then correcting time zero. Global analysis was conducted for identifying initial

DOI: 10.1021/jacs.8b05834
J. Am. Chem. Soc. 2018, 140, 9996−10008

overlapping spectral features and kinetics, by decomposing principle spectra and kinetics using Surface Xplorer software (Ultrafast Systems) with the corrected spectra in narrow wavelength range covering desired signals.

Morphological Characterization. Grazing-incidence wide-angle X-ray scattering (GIWAXS)[95] was used to investigate the molecular packing and crystalline properties. 2D GIWAXS data were acquired at beamline 7.3.3 at the Advanced Light Source, LBNL. Data were acquired just above the critical angle (~0.13°) of the films with a hard X-ray energy of 10 keV. Ag Behenate (AgB) was used for geometry calibration. R-SoXS[96] measurements were performed at the beamline 11.0.1.2, Advanced Light Source (ALS), Lawrence Berkeley National Laboratory, following the previously established protocols. R-SoXS was performed in a transmission geometry with linearly polarized photons under high vacuum (1×10^{-7} Torr) and a cooled (−45 °C) CCD (Princeton PI-MTE, 2048 × 2048 pixels) was used to capture the soft X-ray scattering 2D maps and PS300 was used for geometry calibration. The raw 2D X-ray data were processed with a modified version of NIKA into 1D scattering profiles I(q).

■ ASSOCIATED CONTENT

Supporting Information

The Supporting Information is available free of charge on the ACS Publications website at DOI: 10.1021/jacs.8b05834.

Details regarding the analysis of optoelectronic device measurements, modeling, and analysis of time-resolved and steady state photoluminescence spectroscopy and transient absorption spectroscopy, additional characterization of FIDTT-2PDI and PCE10, and synthesis of FIDTT-2PDI (PDF)

■ AUTHOR INFORMATION

Corresponding Authors

*ajen@uw.edu

*dginger@uw.edu

ORCID

Mark E. Ziffer: 0000-0003-2324-3876

Sae Byeok Jo: 0000-0001-7383-3546

Long Ye: 0000-0002-5884-0083

Hongbin Liu: 0000-0001-9011-1182

Xiaosong Li: 0000-0001-7341-6240

Harald W. Ade: 0000-0002-7871-1158

Alex K.-Y. Jen: 0000-0002-9219-7749

David S. Ginger: 0000-0002-9759-5447

Author Contributions

#S.B.J. and M.E.Z. contributed equally to this work

Notes

The authors declare no competing financial interest.

■ ACKNOWLEDGMENTS

S.B.J. and M.E.Z. contributed equally to this work. This work was supported by the Office of Naval Research through grant number N00014-17-1-2201 (M.E.Z., S.B.J., H.Z., F.L., J.Z., A.K.-Y.J., D.S.G.). Part of this work was conducted at the Molecular Analysis Facility, a National Nanotechnology Coordinated Infrastructure site at the University of Washington which is supported in part by the National Science Foundation (grant ECC-1542101), the University of Washington, the Molecular Engineering & Sciences Institute, and the Clean Energy Institute. Crystallographic studies were carried out at the beamlines 11.0.1.2 and 7.3.3, Advanced Light Source, Lawrence Berkeley National Laboratory, which is supported by U.S. Department of Energy under contract DE-AC02-05CH11231. L.Y. and H.A. were supported by Office of Naval Research (ONR, Grant Nos. N00141412322 and N00141712204). Theoretical research by H.L. and X.L. was supported by the National Science Foundation (CHE-1565520 to X.L.). The use of advanced computational, storage, and networking infrastructure was provided by the Hyak supercomputer system and was funded by the STF at the University of Washington and the National Science Foundation (MRI-1624430).

■ REFERENCES

(1) Shockley, W.; Queisser, H. J. *J. Appl. Phys.* **1961**, *32* (3), 510−519.

(2) Rau, U. *Phys. Rev. B: Condens. Matter Mater. Phys.* **2007**, *76* (8), 085303.

(3) Würfel, P. *Physics of Solar Cells*; Wiley-VCH: Weinheim, 2005.

(4) Miller, O. D.; Yablonovitch, E.; Kurtz, S. R. *IEEE J. of Photovolt.* **2012**, *2* (3), 303−311.

(5) Green, M. A. *Prog. Photovoltaics* **2012**, *20* (4), 472−476.

(6) Abdi-Jalebi, M.; Andaji-Garmaroudi, Z.; Cacovich, S.; Stavrakas, C.; Philippe, B.; Richter, J. M.; Alsari, M.; Booker, E. P.; Hutter, E. M.; Pearson, A. J.; Lilliu, S.; Savenije, T. J.; Rensmo, H.; Divitini, G.; Ducati, C.; Friend, R. H.; Stranks, S. D. *Nature* **2018**, *555* (7697), 497−501.

(7) Baran, D.; Kirchartz, T.; Wheeler, S.; Dimitrov, S.; Abdelsamie, M.; Gorman, J.; Ashraf, R. S.; Holliday, S.; Wadsworth, A.; Gasparini, N.; Kaienburg, P.; Yan, H.; Amassian, A.; Brabec, C. J.; Durrant, J. R.; McCulloch, I. *Energy Environ. Sci.* **2016**, *9* (12), 3783−3793.

(8) Liu, J.; Chen, S.; Qian, D.; Gautam, B.; Yang, G.; Zhao, J.; Bergqvist, J.; Zhang, F.; Ma, W.; Ade, H.; Inganäs, O.; Gundogdu, K.; Gao, F.; Yan, H. *Nat. Energy* **2016**, *1* (7), 16089.

(9) Vandewal, K.; Tvingstedt, K.; Gadisa, A.; Inganas, O.; Manca, J. V. *Nat. Mater.* **2009**, *8* (11), 904−9.

(10) Tvingstedt, K.; Vandewal, K.; Gadisa, A.; Zhang, F.; Manca, J.; Inganas, O. *J. Am. Chem. Soc.* **2009**, *131* (33), 11819−24.

(11) Jailaubekov, A. E.; Willard, A. P.; Tritsch, J. R.; Chan, W. L.; Sai, N.; Gearba, R.; Kaake, L. G.; Williams, K. J.; Leung, K.; Rossky, P. J.; Zhu, X. Y. *Nat. Mater.* **2013**, *12* (1), 66−73.

(12) Vandewal, K.; Albrecht, S.; Hoke, E. T.; Graham, K. R.; Widmer, J.; Douglas, J. D.; Schubert, M.; Mateker, W. R.; Bloking, J. T.; Burkhard, G. F.; Sellinger, A.; Frechet, J. M.; Amassian, A.; Riede, M. K.; McGehee, M. D.; Neher, D.; Salleo, A. *Nat. Mater.* **2014**, *13* (1), 63−8.

(13) Rao, A.; Chow, P. C.; Gelinas, S.; Schlenker, C. W.; Li, C. Z.; Yip, H. L.; Jen, A. K.; Ginger, D. S.; Friend, R. H. *Nature* **2013**, *500* (7463), 435−9.

(14) Bakulin, A. A.; Rao, A.; Pavelyev, V. G.; van Loosdrecht, P. H.; Pshenichnikov, M. S.; Niedzialek, D.; Cornil, J.; Beljonne, D.; Friend, R. H. *Science* **2012**, *335* (6074), 1340−4.

(15) Burke, T. M.; Sweetnam, S.; Vandewal, K.; McGehee, M. D. *Adv. Energy Mater.* **2015**, *5* (11), 1500123.

(16) Sariciftci, N. S.; Smilowitz, L.; Heeger, A. J.; Wudl, F. *Science* **1992**, *258* (5087), 1474−6.

(17) Halls, J. J. M.; Walsh, C. A.; Greenham, N. C.; Marseglia, E. A.; Friend, R. H.; Moratti, S. C.; Holmes, A. B. *Nature* **1995**, *376* (6540), 498−500.

(18) Sun, Y. P.; Bunker, C. E. *J. Phys. Chem.* **1993**, *97* (26), 6770−6773.

(19) Chen, X.-K.; Brédas, J.-L. *Adv. Energy Mater.* **2018**, *8* (9), 1702227.

(20) Benduhn, J.; Tvingstedt, K.; Piersimoni, F.; Ullbrich, S.; Fan, Y.; Tropiano, M.; McGarry, K. A.; Zeika, O.; Riede, M. K.; Douglas, C. J.; Barlow, S.; Marder, S. R.; Neher, D.; Spoltore, D.; Vandewal, K. *Nat. Energy* **2017**, *2* (6), 17053.

(21) Yao, J.; Kirchartz, T.; Vezie, M. S.; Faist, M. A.; Gong, W.; He, Z.; Wu, H.; Troughton, J.; Watson, T.; Bryant, D.; Nelson, J. *Phys. Rev. Appl.* **2015**, *4* (1), 014020.

DOI: 10.1021/jacs.8b05834
J. Am. Chem. Soc. 2018, 140, 9996−10008

(22) Rau, U.; Blank, B.; Müller, T. C. M.; Kirchartz, T. *Phys. Rev. Appl.* **2017**, *7* (4), 044016.
(23) Chen, X.-K.; Ravva, M. K.; Li, H.; Ryno, S. M.; Brédas, J.-L. *Adv. Energy Mater.* **2016**, *6* (24), 1601325.
(24) Yan, C.; Barlow, S.; Wang, Z.; Yan, H.; Jen, A. K. Y.; Marder, S. R.; Zhan, X. *Nat. Rev. Mater.* **2018**, *3* (3), 18003.
(25) Sun, J.; Ma, X.; Zhang, Z.; Yu, J.; Zhou, J.; Yin, X.; Yang, L.; Geng, R.; Zhu, R.; Zhang, F.; Tang, W. *Adv. Mater.* **2018**, *30* (16), 1707150.
(26) Xu, X.; Yu, T.; Bi, Z.; Ma, W.; Li, Y.; Peng, Q. *Adv. Mater.* **2018**, *30* (3), 1703973.
(27) Yao, Z.; Liao, X.; Gao, K.; Lin, F.; Xu, X.; Shi, X.; Zuo, L.; Liu, F.; Chen, Y.; Jen, A. K. *J. Am. Chem. Soc.* **2018**, *140* (6), 2054−2057.
(28) Shi, X.; Zuo, L.; Jo, S. B.; Gao, K.; Lin, F.; Liu, F.; Jen, A. K. Y. *Chem. Mater.* **2017**, *29* (19), 8369−8376.
(29) Dai, S.; Zhao, F.; Zhang, Q.; Lau, T. K.; Li, T.; Liu, K.; Ling, Q.; Wang, C.; Lu, X.; You, W.; Zhan, X. *J. Am. Chem. Soc.* **2017**, *139* (3), 1336−1343.
(30) Li, S.; Ye, L.; Zhao, W.; Yan, H.; Yang, B.; Liu, D.; Li, W.; Ade, H.; Hou, J. *J. Am. Chem. Soc.* **2018**, *140* (23), 7159−7167.
(31) Pope, M.; Swenberg, C. E. *Electronic Processes in Organic Crystals and Polymers*, 2nd ed.; Oxford University Press: New York, 1999.
(32) Goushi, K.; Yoshida, K.; Sato, K.; Adachi, C. *Nat. Photonics* **2012**, *6* (4), 253−258.
(33) Chen, X. K.; Tsuchiya, Y.; Ishikawa, Y.; Zhong, C.; Adachi, C.; Bredas, J. L. *Adv. Mater.* **2017**, *29* (46), 1702767.
(34) Cotts, B. L.; McCarthy, D. G.; Noriega, R.; Penwell, S. B.; Delor, M.; Devore, D. D.; Mukhopadhyay, S.; De Vries, T. S.; Ginsberg, N. S. *ACS Energy Lett.* **2017**, *2* (7), 1526−1533.
(35) Vandewal, K. *Annu. Rev. Phys. Chem.* **2016**, *67*, 113−33.
(36) Kirchartz, T.; Pieters, B. E.; Taretto, K.; Rau, U. *Phys. Rev. B: Condens. Matter Mater. Phys.* **2009**, *80* (3), 035334.
(37) Knesting, K. M.; Ju, H.; Schlenker, C. W.; Giordano, A. J.; Garcia, A.; Smith, O. N. L.; Olson, D. C.; Marder, S. R.; Ginger, D. S. *J. Phys. Chem. Lett.* **2013**, *4* (23), 4038−4044.
(38) Ok, K. H.; Kim, J.; Park, S. R.; Kim, Y.; Lee, C. J.; Hong, S. J.; Kwak, M. G.; Kim, N.; Han, C. J.; Kim, J. W. *Sci. Rep.* **2015**, *5*, 9464.
(39) Han, G.; Guo, Y.; Song, X.; Wang, Y.; Yi, Y. *J. Mater. Chem. C* **2017**, *5* (20), 4852−4857.
(40) Ren, G.; Schlenker, C. W.; Ahmed, E.; Subramaniyan, S.; Olthof, S.; Kahn, A.; Ginger, D. S.; Jenekhe, S. A. *Adv. Funct. Mater.* **2013**, *23* (10), 1238−1249.
(41) Cho, M. J.; Park, G. E.; Park, S. Y.; Kim, Y.-U.; Choi, D. H. *RSC Adv.* **2017**, *7* (62), 38773−38779.
(42) Li, S.; Liu, W.; Li, C.-Z.; Lau, T.-K.; Lu, X.; Shi, M.; Chen, H. *J. Mater. Chem. A* **2016**, *4* (39), 14983−14987.
(43) Vandewal, K.; Tvingstedt, K.; Gadisa, A.; Inganäs, O.; Manca, J. V. *Phys. Rev. B: Condens. Matter Mater. Phys.* **2010**, *81* (12), 125204.
(44) Gong, W.; Faist, M. A.; Ekins-Daukes, N. J.; Xu, Z.; Bradley, D. D. C.; Nelson, J.; Kirchartz, T. *Phys. Rev. B: Condens. Matter Mater. Phys.* **2012**, *86* (2), 024201.
(45) Di Nuzzo, D.; Wetzelaer, G.-J. A. H.; Bouwer, R. K. M.; Gevaerts, V. S.; Meskers, S. C. J.; Hummelen, J. C.; Blom, P. W. M.; Janssen, R. A. J. *Adv. Energy Mater.* **2013**, *3* (1), 85−94.
(46) Veldman, D.; Meskers, S. C. J.; Janssen, R. A. J. *Adv. Funct. Mater.* **2009**, *19* (12), 1939−1948.
(47) Partee, J.; Frankevich, E. L.; Uhlhorn, B.; Shinar, J.; Ding, Y.; Barton, T. J. *Phys. Rev. Lett.* **1999**, *82* (18), 3673−3676.
(48) Rothe, C.; Monkman, A. P. *Phys. Rev. B: Condens. Matter Mater. Phys.* **2003**, *68* (7), 075208.
(49) Hertel, D.; Bässler, H.; Guentner, R.; Scherf, U. *J. Chem. Phys.* **2001**, *115* (21), 10007−10013.
(50) Romanovskii, Y. V.; Gerhard, A.; Schweitzer, B.; Scherf, U.; Personov, R. I.; Bassler, H. *Phys. Rev. Lett.* **2000**, *84* (5), 1027−30.
(51) Hertel, D.; Setayesh, S.; Nothofer, H. G.; Scherf, U.; Müllen, K.; Bässler, H. *Adv. Mater.* **2001**, *13* (1), 65−70.
(52) Theander, M.; Yartsev, A.; Zigmantas, D.; Sundström, V.; Mammo, W.; Andersson, M. R.; Inganäs, O. *Phys. Rev. B: Condens. Matter Mater. Phys.* **2000**, *61* (19), 12957−12963.
(53) Shaw, P. E.; Ruseckas, A.; Samuel, I. D. W. *Adv. Mater.* **2008**, *20* (18), 3516−3520.
(54) Hedley, G. J.; Ward, A. J.; Alekseev, A.; Howells, C. T.; Martins, E. R.; Serrano, L. A.; Cooke, G.; Ruseckas, A.; Samuel, I. D. *Nat. Commun.* **2013**, *4*, 2867.
(55) Arndt, A. P.; Gerhard, M.; Quintilla, A.; Howard, I. A.; Koch, M.; Lemmer, U. *J. Phys. Chem. C* **2015**, *119* (24), 13516−13523.
(56) Gerhard, M.; Arndt, A. P.; Howard, I. A.; Rahimi-Iman, A.; Lemmer, U.; Koch, M. *J. Phys. Chem. C* **2015**, *119* (51), 28309−28318.
(57) Jarzab, D.; Cordella, F.; Gao, J.; Scharber, M.; Egelhaaf, H.-J.; Loi, M. A. *Adv. Energy Mater.* **2011**, *1* (4), 604−609.
(58) Morteani, A. C.; Sreearunothai, P.; Herz, L. M.; Friend, R. H.; Silva, C. *Phys. Rev. Lett.* **2004**, *92* (24), 247402.
(59) Gélinas, S.; Paré-Labrosse, O.; Brosseau, C.-N.; Albert-Seifried, S.; McNeill, C. R.; Kirov, K. R.; Howard, I. A.; Leonelli, R.; Friend, R. H.; Silva, C. *J. Phys. Chem. C* **2011**, *115* (14), 7114−7119.
(60) Keivanidis, P. E.; Kamm, V.; Dyer-Smith, C.; Zhang, W.; Laquai, F.; McCulloch, I.; Bradley, D. D.; Nelson, J. *Adv. Mater.* **2010**, *22* (45), 5183−7.
(61) Keivanidis, P. E.; Kamm, V.; Zhang, W.; Floudas, G.; Laquai, F.; McCulloch, I.; Bradley, D. D. C.; Nelson, J. *Adv. Funct. Mater.* **2012**, *22* (11), 2318−2326.
(62) Huang, Y. S.; Westenhoff, S.; Avilov, I.; Sreearunothai, P.; Hodgkiss, J. M.; Deleener, C.; Friend, R. H.; Beljonne, D. *Nat. Mater.* **2008**, *7* (6), 483−9.
(63) Veldman, D.; Ipek, O.; Meskers, S. C.; Sweelssen, J.; Koetse, M. M.; Veenstra, S. C.; Kroon, J. M.; van Bavel, S. S.; Loos, J.; Janssen, R. A. *J. Am. Chem. Soc.* **2008**, *130* (24), 7721−35.
(64) Bernardo, B.; Cheyns, D.; Verreet, B.; Schaller, R. D.; Rand, B. P.; Giebink, N. C. *Nat. Commun.* **2014**, *5*, 3245.
(65) Loi, M. A.; Toffanin, S.; Muccini, M.; Forster, M.; Scherf, U.; Scharber, M. *Adv. Funct. Mater.* **2007**, *17* (13), 2111−2116.
(66) Howard, I. A.; Mauer, R.; Meister, M.; Laquai, F. *J. Am. Chem. Soc.* **2010**, *132* (42), 14866−76.
(67) Bartesaghi, D.; Perez, I. d. C.; Kniepert, J.; Roland, S.; Turbiez, M.; Neher, D.; Koster, L. J. *Nat. Commun.* **2015**, *6*, 7083.
(68) Etzold, F.; Howard, I. A.; Mauer, R.; Meister, M.; Kim, T. D.; Lee, K. S.; Baek, N. S.; Laquai, F. *J. Am. Chem. Soc.* **2011**, *133* (24), 9469−79.
(69) Shuttle, C. G.; O'Regan, B.; Ballantyne, A. M.; Nelson, J.; Bradley, D. D. C.; Durrant, J. R. *Phys. Rev. B: Condens. Matter Mater. Phys.* **2008**, *78* (11), 113201.
(70) Keivanidis, P. E.; Ho, P. K. H.; Friend, R. H.; Greenham, N. C. *Adv. Funct. Mater.* **2010**, *20* (22), 3895−3903.
(71) Ye, L.; Hu, H.; Ghasemi, M.; Wang, T.; Collins, B. A.; Kim, J.-H.; Jiang, K.; Carpenter, J. H.; Li, H.; Li, Z.; McAfee, T.; Zhao, J.; Chen, X.; Lai, J. L. Y.; Ma, T.; Bredas, J.-L.; Yan, H.; Ade, H. *Nat. Mater.* **2018**, *17* (3), 253−260.
(72) Zhong, H.; Li, C.-Z.; Carpenter, J.; Ade, H.; Jen, A. K. Y. *J. Am. Chem. Soc.* **2015**, *137* (24), 7616−7619.
(73) Kronemeijer, A. J.; Pecunia, V.; Venkateshvaran, D.; Nikolka, M.; Sadhanala, A.; Moriarty, J.; Szumilo, M.; Sirringhaus, H. *Adv. Mater.* **2014**, *26* (5), 728−33.
(74) Graham, K. R.; Cabanetos, C.; Jahnke, J. P.; Idso, M. N.; El Labban, A.; Ngongang Ndjawa, G. O.; Heumueller, T.; Vandewal, K.; Salleo, A.; Chmelka, B. F.; Amassian, A.; Beaujuge, P. M.; McGehee, M. D. *J. Am. Chem. Soc.* **2014**, *136* (27), 9608−18.
(75) Zhao, W.; Qian, D.; Zhang, S.; Li, S.; Inganas, O.; Gao, F.; Hou, J. *Adv. Mater.* **2016**, *28* (23), 4734−9.
(76) Vandewal, K.; Benduhn, J.; Schellhammer, K. S.; Vangerven, T.; Ruckert, J. E.; Piersimoni, F.; Scholz, R.; Zeika, O.; Fan, Y.; Barlow, S.; Neher, D.; Marder, S. R.; Manca, J.; Spoltore, D.; Cuniberti, G.; Ortmann, F. *J. Am. Chem. Soc.* **2017**, *139* (4), 1699−1704.
(77) Burke, T. M.; McGehee, M. D. *Adv. Mater.* **2014**, *26* (12), 1923−1928.

DOI: 10.1021/jacs.8b05834
J. Am. Chem. Soc. 2018, 140, 9996−10008

(78) Sweetnam, S.; Graham, K. R.; Ngongang Ndjawa, G. O.; Heumüller, T.; Bartelt, J. A.; Burke, T. M.; Li, W.; You, W.; Amassian, A.; McGehee, M. D. *J. Am. Chem. Soc.* **2014**, *136* (40), 14078−14088.
(79) Ndjawa, G. O. N.; Graham, K. R.; Mollinger, S.; Wu, D. M.; Hanifi, D.; Prasanna, R.; Rose, B. D.; Dey, S.; Yu, L.; Brédas, J. L.; McGehee, M. D.; Salleo, A.; Amassian, A. *Adv. Energy Mater.* **2017**, *7* (12), 1601995.
(80) Sini, G.; Schubert, M.; Risko, C.; Roland, S.; Lee, O. P.; Chen, Z.; Richter, T. V.; Dolfen, D.; Coropceanu, V.; Ludwigs, S.; Scherf, U.; Facchetti, A.; Fréchet, J. M. J.; Neher, D. *Adv. Energy Mater.* **2018**, *8* (12), 1702232.
(81) Ran, N. A.; Love, J. A.; Takacs, C. J.; Sadhanala, A.; Beavers, J. K.; Collins, S. D.; Huang, Y.; Wang, M.; Friend, R. H.; Bazan, G. C.; Nguyen, T. Q. *Adv. Mater.* **2016**, *28* (7), 1482−8.
(82) Tamai, Y.; Fan, Y.; Kim, V. O.; Ziabrev, K.; Rao, A.; Barlow, S.; Marder, S. R.; Friend, R. H.; Menke, S. M. *ACS Nano* **2017**, *11* (12), 12473−12481.
(83) Szarko, J. M.; Rolczynski, B. S.; Lou, S. J.; Xu, T.; Strzalka, J.; Marks, T. J.; Yu, L.; Chen, L. X. *Adv. Funct. Mater.* **2014**, *24* (1), 10−26.
(84) Cha, H.; Wheeler, S.; Holliday, S.; Dimitrov, S. D.; Wadsworth, A.; Lee, H. H.; Baran, D.; McCulloch, I.; Durrant, J. R. *Adv. Funct. Mater.* **2018**, *28* (3), 1704389.
(85) Li, Y.; Zhong, L.; Gautam, B.; Bin, H.-J.; Lin, J.-D.; Wu, F.-P.; Zhang, Z.; Jiang, Z.-Q.; Zhang, Z.-G.; Gundogdu, K.; Li, Y.; Liao, L.-S. *Energy Environ. Sci.* **2017**, *10* (7), 1610−1620.
(86) Zheng, Z.; Awartani, O. M.; Gautam, B.; Liu, D.; Qin, Y.; Li, W.; Bataller, A.; Gundogdu, K.; Ade, H.; Hou, J. *Adv. Mater.* **2017**, *29* (5), 1604241.
(87) Gélinas, S.; Rao, A.; Kumar, A.; Smith, S. L.; Chin, A. W.; Clark, J.; van der Poll, T. S.; Bazan, G. C.; Friend, R. H. *Science* **2014**, *343* (6170), 512−516.
(88) Zhang, J.; Gu, Q.; Do, T. T.; Rundel, K.; Sonar, P.; Friend, R. H.; McNeill, C. R.; Bakulin, A. A. *J. Phys. Chem. A* **2018**, *122* (5), 1253−1260.
(89) Jakowetz, A. C.; Böhm, M. L.; Zhang, J.; Sadhanala, A.; Huettner, S.; Bakulin, A. A.; Rao, A.; Friend, R. H. *J. Am. Chem. Soc.* **2016**, *138* (36), 11672−11679.
(90) Gorenflot, J.; Paulke, A.; Piersimoni, F.; Wolf, J.; Kan, Z.; Cruciani, F.; Labban, A. E.; Neher, D.; Beaujuge, P. M.; Laquai, F. *Adv. Energy Mater.* **2018**, *8* (4), 1701678.
(91) Katahara, J. K.; Hillhouse, H. W. *J. Appl. Phys.* **2014**, *116* (17), 173504.
(92) Braly, I. L.; deQuilettes, D. W.; Pazos-Outón, L. M.; Burke, S.; Ziffer, M. E.; Ginger, D. S.; Hillhouse, H. W. *Nat. Photonics* **2018**, *12* (6), 355−361.
(93) Forrest, S. R.; Bradley, D. D. C.; Thompson, M. E. *Adv. Mater.* **2003**, *15* (13), 1043−1048.
(94) de Mello, J. C.; Wittmann, H. F.; Friend, R. H. *Adv. Mater.* **1997**, *9* (3), 230−232.
(95) Hexemer, A.; Bras, W.; Glossinger, J.; Schaible, E.; Gann, E.; Kirian, R.; MacDowell, A.; Church, M.; Rude, B.; Padmore, H. *Conference Series* **2010**, *247* (1), 012007.
(96) Gann, E.; Young, A. T.; Collins, B. A.; Yan, H.; Nasiatka, J.; Padmore, H. A.; Ade, H.; Hexemer, A.; Wang, C. *Rev. Sci. Instrum.* **2012**, *83* (4), 045110.

DOI: 10.1021/jacs.8b05834
J. Am. Chem. Soc. 2018, 140, 9996−10008